World Conference on Timber Engineering Oslo 2023

EVALUATION OF SEISMIC PERFORMANCE FACTORS AND FRAGILITY FUNCTIONS FOR POST-TENSIONED MASS PLY PANEL ROCKING WALLS

Tu X. Ho[1], Patricio Uarac P.[2], Andre R. Barbosa [3], Arijit Sinha[4], Barbara Simpson[5], Gustavo A. Araújo R.[6], Gustavo F. Orozco[7]

ABSTRACT: This paper presents the statistical and numerical investigation of the seismic performance of a three-story post-tensioned mass ply panel (MPP) rocking wall lateral force-resisting system prototype whose main components are MPP, U-shaped flexural steel plates (UFPs), and high-strength steel post-tensioned rods. Uncertainties in material properties and geometry of the components are considered in the assessment of the performance of this lateral force-resisting system based on recent experimental data on MPP, experimental data available in the literature for the UFPs and post-tensioning rods, as well as some additional structural design considerations. In the assessment of the seismic performance factors, first, random realizations of the structural design are generated using Monte Carlo simulation. Second, for each realization, a nonlinear finite element model is developed. For each realization, two types of analysis are performed, nonlinear static analyses, and incremental dynamic analyses. Results of the nonlinear static and dynamic analyses are then used to estimate the seismic design factors (e.g., R-factor) and limit state-based fragility functions, the latter being based on exceeding limit states defined for each component based on existing experimental data.

KEYWORDS: Fragility function, incremental dynamic analysis, mass ply panel, post-tensioned rocking wall, pushover analysis, R-factor.

1 INTRODUCTION

Mass timber materials have gained public attention and are finding expanded uses in the building sector. The International Building Code [1] introduced new building types in the last code revision cycle, which now allows for the design and construction of mass timber buildings up to 18 stories tall. Innovative lateral force-resisting systems (LFRS), such as post-tensioned rocking walls coupled with different energy dissipation solutions, have been designed for use in buildings per (i) the equivalent lateral force procedure in ASCE 7 [2] assuming a conservative seismic response modification coefficient (R-factor) [3], or (ii) state-of-the-art performance-based design methods requiring the use of alternative means and methods of design and analysis, which were mentioned by FEMA P-58 [4]. However, even though a few buildings have been built using these LFRS [5], few studies have focused on the seismic performance of mass timber post-tensioned rocking walls, and therefore, the seismic design factors (e.g., R-factor) of the system, which is used in ASCE 7 and other seismic design standards, and fragility functions needed to fully adopt the FEMA P-58 methodology have been based on expert judgement [6] that have been largely conservative. Based on existing knowledge and recent experimental test data, this paper summarizes the nonlinear modelling of post-tensioned mass ply panel (MPP) rocking walls coupled with U-shaped flexural plates (UFPs) and presents the seismic performance assessment of a three-story building adopting this LFRS [7]. Effects of epistemic and aleatory uncertainties were explicitly accounted for in the seismic performance assessment of the rocking wall system, following a validated method available in the literature [8]. Results of the nonlinear analyses are presented in terms of collapse fragility functions and seismic performance factors, which may be used as a first step in the determination of low- and mid-rise building archetypes consisting of post-tensioned mass timber walls.

[1] Tu X. Ho, Department of Wood Science and Engineering, Oregon State University, tu.ho@oregonstate.edu
[2] Patricio Uarac P., School of Civil and Construction Engineering, Oregon State University, uaracpip@oregonstate.edu
[3] Andre R. Barbosa, School of Civil and Construction Engineering, Oregon State University, andre.barbosa@oregonstate.edu
[4] Arijit Sinha, Department of Wood Science and Engineering, Oregon State University, arijit.sinha@oregonstate.edu
[5] Barbara Simpson, Department of Civil and Environmental Engineering, Stanford University, bsimpson@stanford.edu
[6] Gustavo A. Araújo R., Department of Civil and Environmental Engineering, Stanford University, garaujor@stanford.edu
[7] Gustavo F. Orozco, School of Civil and Construction Engineering, Oregon State University, gustavo.orozco@oregonstate.edu

https://doi.org/10.52202/069179-0337

2 METHODOLOGY

2.1 DESCRIPTION OF STRUCTURE

The LFRS was designed for an occupancy consistent with that of an office building archetype located at a site in Seattle, Washington, USA with soil class D and seismic response spectral values, S_{DS} = 0.97 g, S_{D1} = 0.61 g. The direct displacement-based design (DDBD) method [9]–[11] was used for the design of the LFRS. The design base shear was determined by using the capacity spectrum approach [9] and was utilized to design shear wall dimensions, UFPs, and high-strength post-tensioned rods. In the design, a flag shape hysteretic model [11] was utilized to estimate the effective damping of the post-tensioned rocking wall, assuming a damping ratio of 10%. The LFRS was designed to meet requirements of three performance levels [Immediate Occupancy (IO), Life Safety (LS), and Collapse Prevention (CP)], each corresponding to an earthquake hazard intensity level [Service Level Earthquake (SLE), Design Earthquake (DE), and risk-targeted Maximum Considered Earthquake (MCE_R), respectively]. Table 1 lists the performance targets for each performance level. The targets are defined in terms of peak inter-story drift (D_{max}), strains in the post-tensioning rods (ε_{PTmax}), and MPP compression strains at the rocking interface (ε_{MPPmax}). The thresholds strains for the post-tensioning rods and MPP wall are defined such that they remain in the elastic range at IO and LS levels, while both tension rods and MPP are allowed to yield at CP level, but without exceeding their ultimate strains in tension and compression, respectively.

Table 1: *Performance levels and targets*

Performance Level	EQ Levels	Performance thresholds		
		D_{max}	ε_{PTmax}	ε_{MPPmax}
IO	SLE	1.0%	0.0044	0.0032
LS	DE	2.0%	0.0044	0.0032
CP	MCE_R	4.0%	0.0066	0.0075

The investigated post-tensioned rocking wall LFRS shown in Figure 1 (UFP wall) consists of an MPP shear wall (9144 mm × 2134 mm × 181 mm, F16 wall panel [12]), two pairs of post-tensioning rods (diameter 31.8 mm; ASTM A354 Grade BD [13]) connecting the top of the MPP shear wall to the foundation, and 20 UFP devices (152 mm wide, 12.7 mm thick and 102 mm bending diameter, ASTM A572 Grade 42 [14]). The UFPs are attached to the MPP and steel bounding columns that connect to the foundation. The steel bounding column is designed to remain elastic at MCE_R. The MPP walls are connected to the MPP floor slabs through one shear key at each floor level and two shear keys at its base. The MPP floor slabs are supported by laminated veneer lumber (LVL) beams and columns.

2.2 FINITE ELEMENT MODEL OF STRUCTURE

Two-dimensional (2D) finite element models were developed in OpenSees [15] to characterize the building geometry shown in Figure 1. For the gravity system, elastic beam-column elements (elasticBeamColumn) were used. The elastic beam-column elements were connected to the beam-column joint using zero-length, elastic elements to account for the rotational stiffness of the connection. For the LFRS, the MPP panel itself was modelled using elastic beam-column elements along the height of the building, with nonlinear springs placed between the base of the wall and the foundation to represent the rocking behaviour and any potential inelasticity due to panel crushing and gap opening at the base of the wall. The nonlinear base springs consisted of 19 zero-length, elastic-perfectly plastic (ElasticPPGap) elements that work only in compression, assuming the compression strength in the major direction of the MPP (f_{c_0}) as the elastic limit and considering a plastic hinge length of two times the thickness of the MPP [16]. The springs were located based on the Gauss-Legendre quadrature points along the width of the panel. The UFPs were also modelled with zero-length elements with a force-displacement relation based on the uniaxial material Giuffre-Menegotto-Pinto [17] model. Properties of the UFPs were calibrated to match available numerical models developed using a Ramberg-Osgood material model [18]. Finally, the post-tensioning rods were modelled as trusses with an initial strain based on the design post-tensioning force and a tension-only nonlinear material model. The model of the LFRS is shown graphically in Figure 2.

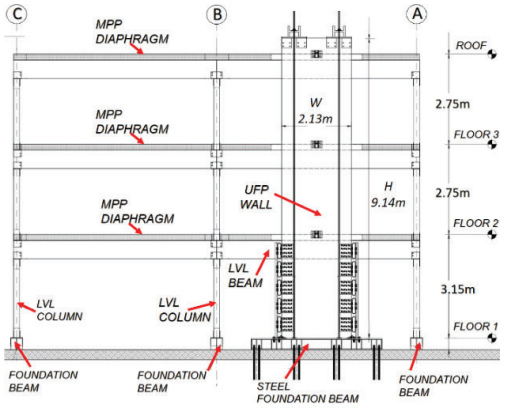

Figure 1: *Elevation of the LFRS archetype*

The finite element models were subjected to nonlinear static pushover analyses and nonlinear time history analyses (NLTHA). For each realization, the fundamental period (T_1) and the associated first-mode shape are computed and used as input parameters for the nonlinear static analysis, where at each floor level, a force is applied following this first-mode distribution with displacement control at the roof level. Each pushover realization is pushed until an 8% roof drift ratio or until is numerically unstable. For the NLTHA, the fundamental period is used to define the target damping ratios for the Rayleigh damping matrix, using committed stiffness and 2% damping associated with the elongated period $1.5T_1$ and short period $0.2T_1$.

https://doi.org/10.52202/069179-0337

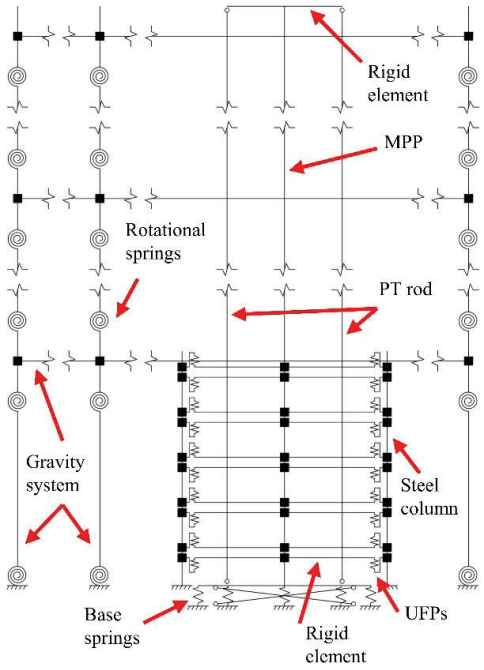

Figure 2: *Finite element model*

2.3 RANDOM VARIABLES AND THEIR STATISTICAL CORRELATIONS

The variability of component properties and dimensions affects the stiffness, strength, and dynamic properties of the structure, and, therefore, its response to loading. Based on the material properties described in this section, a set of 100 structural models were randomly generated. Each model represents a realization of the random variables defining the wall design. Considerations in the model development performed are described in the next subsections.

2.3.1 Material properties

Uncertainties in material properties were based on information available in the literature [19]–[25]. For MPP, Table 2 lists four random variables and their parameters, including mean and coefficients of variation (CoV) for density (ρ_w), modulus of elasticity (E_w), compressive strength in the major direction (f_{c_0}), and shear modulus (G). Expected values were based on the material testing results [24], [25]. Coefficients of variation (CoVs) were determined based on values and formula for glue-laminated timber [22], [23], because currently there is no reliable study on the CoVs of material parameters for MPP, which vary based on base materials, quality control, and material selection schemes implemented in the production of the panels. The density followed a normal distribution while the other properties are lognormally distributed. The four random variables were assumed to be correlated, based on data available for timber materials [22], as shown in Table 3.

Table 2: *Random variables for MPP material properties*

Variable	Dist.	Mean	CoV
ρ_w (kg/m^3)	Normal	34.0	0.10
E_w (MPa)	Lognormal	13626.0	0.13
f_{c_0} (MPa)	Lognormal	44.9	0.12
G (MPa)	Lognormal	509.7	0.13

Table 3: *Correlation coefficient matrix for MPP material properties*

Variable	ρ_w	E_w	$f_{c\ 0}$	G
ρ_w	1.0	0.6	0.8	0.6
E_w	0.6	1.0	0.6	0.6
f_{c0}	0.6	0.6	1.0	0.4
G	0.6	0.6	0.4	1.0

The probabilistic model parameters associated with the mechanical properties of the high-strength rod and other structural steel components are presented in Table 4 and Table 5, respectively. The random variables for the high-strength rods follow a normal distribution, while the structural steel follow lognormal distributions, including the elastic modulus (E_s) and yield strength (f_{sy}) for the UFP components, and on elastic modulus (E_s) and Poisson's ratio (v_s) for the steel bounding columns. The expected values and CoVs were derived from the literature [19], [20].

Table 4: *Random variables for high-strength steel rod properties*

Property	Dist.	Mean	CoV
E_p (GPa)	Normal	200	0.020
f_{pt} (MPa)	Normal	1075.6	0.025
e_u (mm/mm)	Normal	0.05	0.060

Table 5: *Random variables for structural steel properties*

Property	Dist.	Mean	CoV
f_{sy} (MPa)	Lognormal	423	0.105
E_s (GPa)	Lognormal	200	0.045
v_s	Lognormal	0.3	0.045

2.3.2 Component dimensions

Geometric deviations from specified dimensions that also contribute to model uncertainties were accounted for in the probabilistic modelling. For each considered variable, the distribution, mean value, standard deviation, and tolerance are presented in Table 6, where the mean values correspond to the dimensions used for the initial design. Tolerances were considered as the amount by which a measurement might change and still be acceptable [26]; this implies that no realization had geometric values outside the mean plus/minus the tolerance. Values from previous studies were used for the standard deviation and tolerances of each component. For the MPP, standard deviations and tolerances from [27] and [28] were used, respectively. For the UFP thickness, the standard deviation is assumed to be a third of the tolerance from [29]. For the other dimensions, the standard deviation is assumed as half of the tolerance from [30]. For the C-section steel column, the standard deviations are based on [31] and [32], along with tolerances from [30].

https://doi.org/10.52202/069179-0337

Table 6: *Random variables of component dimensions*

Variable	Dist.	Mean [mm]	Std Dev [mm]	Tol. [mm]
Timber panel				
Thickness	Normal	181.0	0.80	1.59
Width	Normal	2133.6	1.59	3.18
Length	Normal	9483.7	3.18	6.35
UFP (Steel Plate)				
Thickness	Lognormal	12.7	0.25	0.76
Width	Normal	152.4	5.56	11.11
Length	Normal	482.6	7.94	15.88
Bending diameter	Normal	88.9	0.89	+0.0 -1.78
C-section steel column				
Depth	Normal	254.0	1.02	+3.18 -2.38
Flange width	Normal	73.4	0.66	+3.18 -3.97
Web thickness	Normal	13.4	0.49	N/A*
Flange thickness	Normal	11.1	0.51	N/A*
High-strength rod				
Diameter	Normal	31.8	0.32	0.25

*N/A: Tolerances not applicable or not available [30].

2.4 PERFORMANCE ASSESSMENT

2.4.1 Damage State Definition

Damage state thresholds were defined using the peak inter-story drift ratio limit as a proxy for damage based on drift limits estimated from component-based (UFP, wall, PT rod, etc.) strain limits developed from experimental data available in the literature. The damage states are associated with the building capacity curve. Three different damage state levels, including Immediate Occupancy (IO), Life Safety (LS), and Collapse Prevention (CP), are defined in this study. The IO damage state is associated with the effective yielding of any components in the building occurs. In the MPP wall LFRS, yielding of UFP devices usually happens at relatively small drift ratios; therefore, yielding of the UFPs is chosen as the indicator of IO damage state in this study. The LS damage state is associated with crushing of the MPP panel or yielding of the PT bar, whichever occurs first. Lastly, the CP damage states are associated with the first occurrence of the following cases: (1) the PT bar strain is greater than the ultimate capacity strain, (2) the peak inter-story drift ratio exceeds 0.1, or (3) the inter-story residual drift is greater than 0.015 [33].

2.4.2 Assessment of the seismic performance factors

The assessment of the seismic performance factors (R-factor, deflection amplification factor, and the over-strength factor) was implemented based on the nonlinear static analyses applied to the set of 100 generated structures. The pushover analysis was used to determine the damage state levels and impact of uncertainties on the R-factor and building capacity. The base shear versus roof drift ratio results were used to obtain the distribution of the building capacity. The mean (μ), mean minus standard deviation (μ-σ), and mean plus standard deviation (μ+σ) of each variable in Figure 3 are determined using the capacity curves. Overall, procedures followed in this study are described in [8] and [34]. The seismic performance factors include: (1) normalized reference yield force, F_y/W, where W is the weight of the structure, (2) reference yield roof drift ratio, d_y/H, where H is the height of the building, (3) displacement ductility factor $\mu = d_u/d_y$ (4) system overstrength factor $\Omega_s = F_y/F_d$, where F_d is the design base shear, and (5) both the seismic modification factor, R, and displacement amplification factor C_d , set equal to the product of the $R_\mu \cdot \Omega_s$., where R_μ is the seismic modification factor associated with the ductility of the system and, thus, set equal to the displacement ductility for this bilinear fitted model.

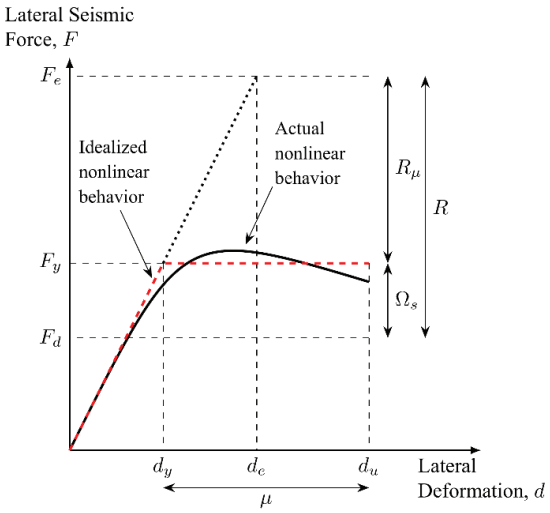

Figure 3: *Equivalent bilinear inelastic model*

2.4.3 Fragility functions

The uncertainties in seismic response were investigated using an incremental dynamic analysis (IDA) for the set of 100 structures. In the IDA, each structure is subjected to the suite of 44 far-field ground motions defined in FEMA P-695 [35]. To reduce computational cost, the 5%-damped response spectral acceleration at the first mode was scaled up to an upper limit of 5g, resulting in a truncated IDA [36]. For each ground motion (GM), increments of 0.2 g were used in the IDA, such that a total of 4,400 IDA was performed. At the IO level, the UFP yielding is chosen as indicator; however, since UFPs reach yielding at relatively small drift ratios, the nonlinear static analysis is used to identify the mean drift ratio where the first-yield of the system occurs, point associated with a 10% drop of the initial stiffness. Using the first-yield drift ratio as threshold on the IDA, a distribution of the amount of UFPs at yielding is obtained and its mean value is used to develop the component fragility function. At CP level, four collapse criteria were used: (1) maximum inter-story drift ratio greater or equal to 0.1, (2) maximum inter-story residual drift ratio greater than 0.015, as recommended by [33], (3) strain in the post-tensioned rods exceeding the maximum strain limit, and (4) numerical non-convergence. As part of the numerical model, the limit states of the UFPs and the MPP panels

https://doi.org/10.52202/069179-0337

were using the uniaxial material 'MinMax' in OpenSees but were not considered a collapse criterion. The use of this 'MinMax' material model means that for strains below or above the ultimate strain of the component, the component fails and returns zero stress.

Based on the IDA results, the fragility functions were fit to a lognormal cumulative distribution function (CDF) with an empirical section and a fitted-extrapolated section, as considered in [37].

3 RESULTS

3.1 SEISMIC PERFORMANCE FACTORS

Figure 4 shows the results of the nonlinear pushover analyses. The results for all 100 structures are shown in grey, while the black curve corresponds to the mean of all the pushover curves. The red line corresponds to a bilinear model calibrated using the Energy Equivalent Elasto-Plastic method [38] fit to the mean pushover curve. A similar calibration process was conducted to obtain the mean plus and minus standard deviation curves (not shown in the figure). Table 7 lists the normalized calibrated factors, reference yield force, and reference yield drift ratio (F_y/W, and d_y/H) for all three calibrated curves. In addition, Table 7 also lists the seismic performance factors. The base shear at the ultimate roof drift ratio of 0.07 represents the lowest force obtained in the mean pushover results.

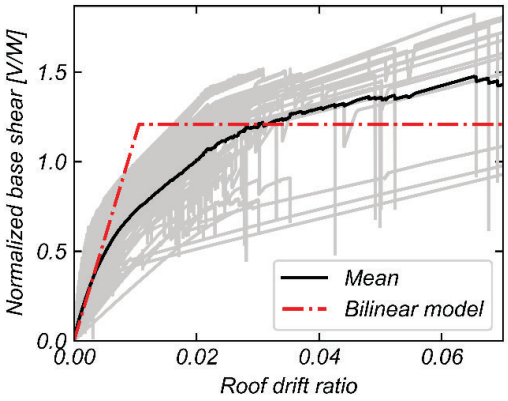

Figure 4: *Pushover results and fitted elastoplastic bilinear model.*

3.2 INCREMENTAL DYNAMIC ANALYSIS (IDA)

Figure 5 shows the results of the IDA, where each grey dot represents the maximum of the absolute peak inter-story drift ratios obtained for each NLTHA for a given realization and ground motion record scaled to the linear elastic, 5%-damped spectral acceleration at the fundamental period of the structure, $S_a(T_1)$. The blue curve represents a typical IDA curve for an individual ground motion and IM_{max} corresponds to the truncated value of the spectral acceleration considered. The mean curve indicates that the LFRS remains essentially elastic up to 0.02 maximum inter-story drift ratio, a soft transition occurs from this point before reaching the plateau of the system around 0.05 maximum inter-story drift ratio associated with IM of 3.3g, which is 3.6 times the S_{DS} value. Note, not all IDA reached the peak inter-story drift ratio of 10%, e.g. at 2%, 4% and 8% of peak inter-story drift ratio, 98%, 79% and 50% of the IDA reached or passed the values respectively.

Table 7: *Seismic performance factor statistics*

Variable	Mean – Std Dev	Mean	Mean + Std Dev
F_y/W	0.95	1.22	1.49
d_y/H	0.0083	0.0122	0.0161
$\mu = R_\mu = d_u/d_y$	4.35	5.74	8.45
$\Omega_s = F_y/F_d$	1.49	1.91	2.34
$R = C_d = R_\mu \cdot \Omega_s$	6.48	11.0	19.8

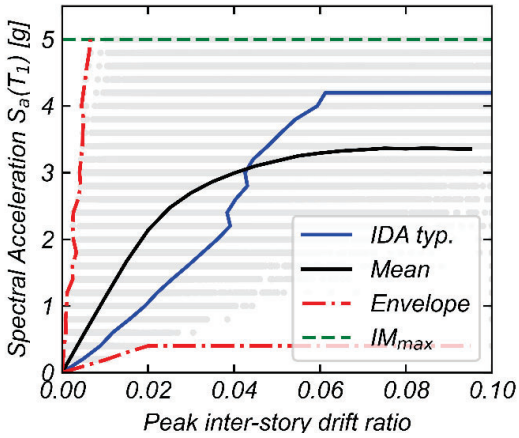

Figure 5: *IDA results for 100 realizations of the structure subjected to 44 FEMA P-695 far-field ground motions.*

As stated on the methodology, at the IO level, the UFPs yield at relatively small drift ratios. From the nonlinear static analysis, it was found that this occurs for an inter-story drift ratio of 0.001 (Figure 4) and the mean first-yield of the system is associated with the yield of one UFP.

Based on the IDA results, for each component, fragility functions were developed in terms of the spectral acceleration versus the normalized peak displacement over the yielding displacement of the UFP (d_u/d_y), normalized maximum stress over the crushing stress of the MPP wall (σ_u/σ_y), and normalized peak strain over the yielding strain on the PT rods ($\varepsilon_u/\varepsilon_y$), which are shown in Figure 6.

https://doi.org/10.52202/069179-0337

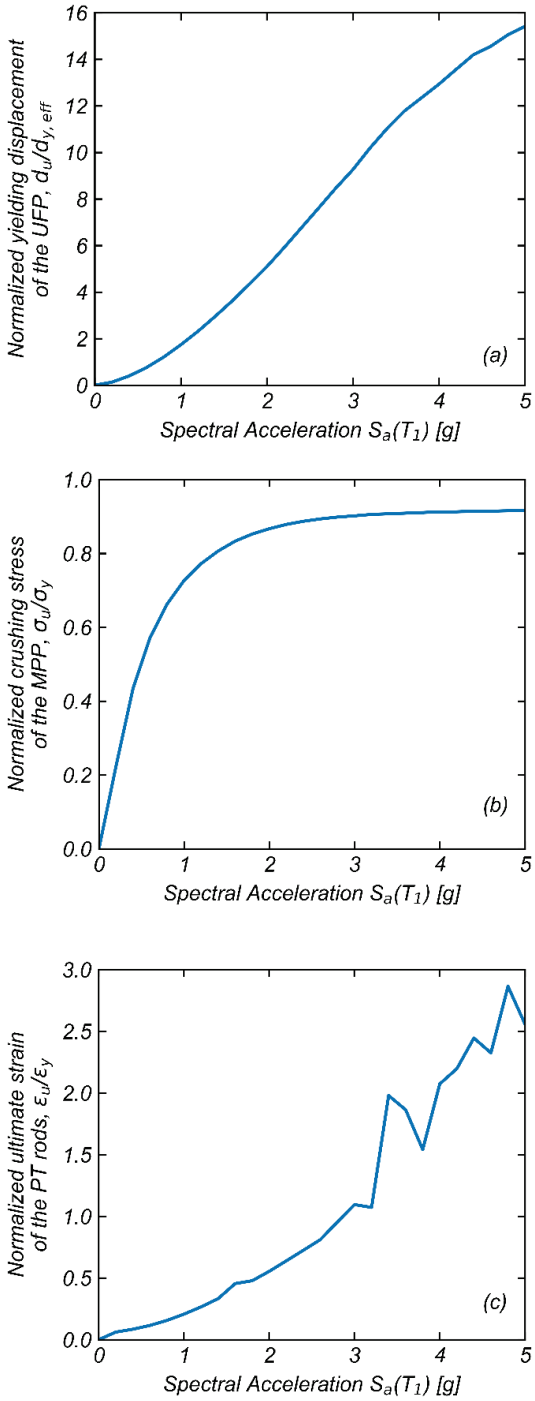

***Figure 6: Mean** empirical component fragility functions for: (a) UFP, (b) MPP panel, (c) PT rod.*

As stated previously, the UFPs reach yielding at small drift ratios compared with peak inter-story drift ratio limit on Table 1 for IO, and similar conclusions can be obtained from the fragility functions, where the IM at yielding is 0.708 g, which is 0.73 times S_{DS}. Between 1 g and 3.5 g, the fragility function is mostly linear and shows a large component displacement ductility of 15.4 at 5 g. The MPP fragility function shows that the MPP wall behaves in the elastic range for all considered IMs, although a plateau forms above 2 g (2.06 times S_{DS}) when the component can no longer resist additional stresses for all limit states. In the case of the PT rod fragility function, the function increases monotonically until yielding at 3 g (3.09 times SDS). After yielding, the function shows abrupt changes that could be related with the snap-back presented in typical IDA.

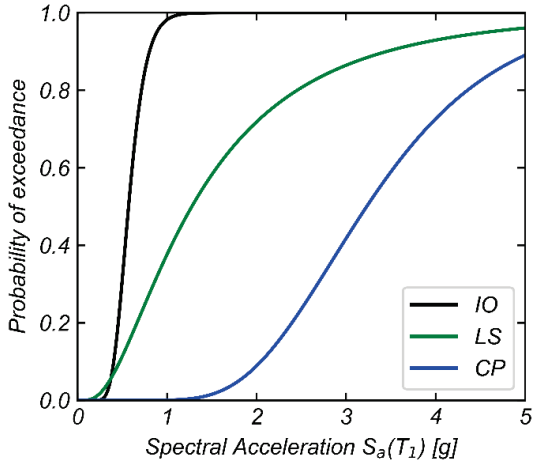

***Figure 7:** Empirical system fragility function for each damage state.*

***Table 8:** IM capacities for different damage states*

	IM		
Damage State	16th percentile	Mean	84th percentile
IO [g]	0.437	0.571	0.744
LS [g]	0.591	1.28	2.76
CP [g]	2.69	3.23	4.60

Table 8 lists the IM for the three damage states considered in this study fitted to a lognormal distribution, the values presented along with the Figure 7 show an overlap of the IO an LS damage for spectral accelerations below 0.5 g which is related to limit states used at each damage state. For IO, the only limit state considered was yield displacement of the UFPs, while for LS either crushing on the MPP or yield of the PT rods were used as limit states. The overlap implies that there is a probability below 5% that the system will sustain damage associated with either IO or LS damage state. Similarly, analysing the components that controls each of these states, UFPs for IO and MPP and PT rods for LS, the larger standard deviation at LS can be attributed to the MPP due its contribution to the nonlinear response at the base spring for each realization, which is a function of the elastic modulus (E_w) and its CoV, which is one order of magnitude greater than the other components. Similarly, at CP, the uncertainties on the MPP play a significant role on the standard deviation of the fragility function.

https://doi.org/10.52202/069179-0337

4 CONCLUSIONS

A statistical and numerical investigation of the seismic performance of post-tensioned MPP rocking walls on a 3-story building is conducted. The uncertainties in material properties of components are considered by generation of the basic random variables to model a set of 100 structures. Nonlinear static analyses and IDA are conducted for each structural realization. From the nonlinear static analysis, the seismic performance factors were estimated. The lower bounds and mean (listed in parentheses) are 6.48 (11.0) for the R-factor, 1.49 (1.91) for the system overstrength, and 4.35 (5.74) for the displacement ductility. From the IDA, empirical component fragility functions were developed as well as system fragility functions for different damage states. The component fragility function shows that the UFPs are the main ductility contributors to the system. The overlap on the system fragility functions for IO and LS damage state shows that there are gaps that must be addressed in the characterization of the uncertainties for mass timber products.

ACKNOWLEDGEMENT

This study is supported by the United States Department of Agriculture (USDA), Agricultural Research Service, Award number: 58-2024-9-165 and by the National Science Foundation (NSF) under award #2120683. We would also like to acknowledge the USDA Agricultural Research Service, the TallWood Design Institute, and our industry partners for supporting this experimental program. Any opinions, findings, and conclusions are those of the authors and do not necessarily reflect views of the supporting agencies.

REFERENCES

[1] International Code Council (IBC), 2021 International Building Code, International Code Council, Inc., 2021.

[2] American Society of Civil Engineers (ASCE), Minimum Design Loads and Associated Criteria for Buildings and Other Structures (ASCE/SEI 7-16). 2017.

[3] A. Busch, R. B. Zimmerman, S. Pei, E. McDonnell, P. Line, D. Huang, Prescriptive Seismic Design Procedure for Post-Tensioned Mass Timber Rocking Walls, *J. Struct. Eng.*, 148(3), 2022.

[4] Applied Technology Council (ATC), Seismic Performance Assessment of Buildings (FEMA P-58), 2018.

[5] E. G. Baas, A. R. Barbosa, M. Riggio, Post-tensioned timber wall buildings: Design & construction practice in New Zealand & United States, *World Conference on Timber Engineering*, 2021.

[6] A. N. Papadopoulos, D. Vamvatsikos, A. K. Kazantzi, Development and Application of FEMA P-58 Compatible Story Loss Functions, *Earthq. Spectra*, 35(1), 95–112, 2019.

[7] G. F. Orozco O., T. X. Ho, G. A. Araújo R., A. R. Barbosa, A. Sinha, B. G. Simpson, Innovative mass timber seismic lateral force resisting systems: Testing of a full-scale three-story building with mass ply panels (MPP) rocking walls, *Proceedings of the 12th National Conference on Earthquake Engineering*, 2022.

[8] L. G. Rodrigues, J. M. Branco, L. A. C. Neves, A. R. Barbosa, Seismic assessment of a heavy-timber frame structure with ring-doweled moment-resisting connections, *Bull. Earthq. Eng.*, 16(3), 1341–1371, 2018.

[9] W. Pang, D. V. Rosowsky, S. Pei, J. W. van de Lindt, Simplified Direct Displacement Design of Six-Story Woodframe Building and Pretest Seismic Performance Assessment, *J. Struct. Eng.*, 136(7), 813–825, 2010.

[10] C. Loss, T. Tannert, S. Tesfamariam, State-of-the-art review of displacement-based seismic design of timber buildings, *Constr. Build. Mater.*, 191, 481–497, 2018.

[11] A. D. Cesare, F. C. Ponzo, S. Pampanin, T. Smith, D. Nigro, N. Lamarucciola, Displacement based design of post-tensioned timber framed buildings with dissipative rocking mechanism, *Soil Dyn. Earthq. Eng.*, 116, 317–330, 2019.

[12] A.-T. E. W. Association, Freres Mass Ply Panels (MPP) and Mass Ply Lam (MPL) Beams and Columns (PR-L325), APA - The Engineered Wood Association, 2022.

[13] ASTM, A354 Standard Specification for Quenched and Tempered Alloy Steel Bolts, Studs, and Other Externally Threaded Fasteners, American Society for Testing and Materials (ASTM) International, 2017.

[14] ASTM, A572/A572M Standard Specification for High-Strength Low-Alloy Columbium-Vanadium Structural Steel, American Society for Testing and Materials (ASTM) International, 2018.

[15] F. McKenna, M. H. Scott, G. L. Fenves, Nonlinear Finite-Element Analysis Software Architecture Using Object Composition, *J. Comput. Civ. Eng.*, 24(1), 95–107, 2010.

[16] T. Akbas *et al.*, Analytical and Experimental Lateral-Load Response of Self-Centering Posttensioned CLT Walls, *J. Struct. Eng.*, 143(6), 2017.

[17] F. C. Filippou, E. P. Popov, V. V. Bertero, Effects of bond deterioration on hysteretic behavior of reinforced concrete joints, 1983.

[18] A. Baird, T. J. Smith, A. Palermo, S. Pampanin, Experimental and numerical Study of U-shape Flexural Plate (UFP) dissipators, *New Zealand Society of Earthquake Engineering*, Mar. 2014. [Online].

[19] J. C. on S. Safety (JCSS), Probabilistic Model Code, Part III - Resistance Models. Section 3.02: Static Properties of Structural Steel (Rolled Sections), 2001.

[20] BS, Hot rolled round steel bars for general purposes - Dimensions and tolerances on shape and dimensions (EN 10060), 2003.

[21] J. C. on S. Safety (JCSS), Probabilistic Model Code, Part III - Resistance Models. Section 3.04: Static Properties of Prestressing Steel (Prestressed Concrete), 2005.

[22] J. C. on S. Safety (JCSS), Probabilistic Model Code, Part III - Resistance Models. Section 3.05: Properties of Timber, 2006,
[23] J. Köhler, J. D. Sørensen, M. H. Faber, Probabilistic modeling of timber structures, *Struct. Saf.*, 29(4), 255–267, 2007.
[24] R. Soti, T. X. Ho, A. Sinha, Structural Performance Characterization of Mass Plywood Panels, *J. Mater. Civ. Eng.*, 33(10), 2021.
[25] T. X. Ho, A. Arora, A. Sinha, In-Plane Shear Properties of Mass Ply Panels in Long-Ply Direction, *J. Mater. Civ. Eng.*, 34(8), 2022.
[26] Cambridge University Press, Cambridge Dictionary: Find Definitions, Meanings & Translations. Accessed: Feb. 24, 2023. [Online].
[27] H. Mpidi Bita, T. Tannert, Disproportionate collapse prevention analysis for a mid-rise flat-plate cross-laminated timber building, *Eng. Struct.*, 178, 460–471, 2019.
[28] APA, ANSI/APA PRG 320: Standard for Performance-Rated Cross-Laminated Timber, 2018. [Online].
[29] P. E. Hess, D. Bruchman, I. A. Assakkaf, B. M. Ayyub, Uncertainties in Material and Geometric Strength and Load Variables, *Nav. Eng. J.*, 114(2), 139–166, 2002.
[30] ASTM, Standard Specification for General Requirements for Rolled Structural Steel Bars, Plates, Shapes, and Sheet Piling (A6-19), 2021.
[31] Z. Kala, J. Melcher, L. Puklický, Material and Geometrical Characteristics Of Structural Steels Based On Statistical Analysis Of Metallurgical Products, *J. Civ. Eng. Manag.*, 15(3), 299–307, 2009.
[32] W. M. Bulleit, Uncertainty in Structural Engineering, *Pract. Period. Struct. Des. Constr.*, 13(1), 24–30, 2008.
[33] Los Angeles Tall Building Structural Design Council, An Alternative Procedure for Seismic Analysis and Design of Tall Buildings Located in the Los Angeles Region, 2020.
[34] J. Varela, J. Tanner, R. Klingner, Development Of Response Modification Coefficient And Deflection Amplification Factor For Design Of Aac Structural Systems, *13th World Conference on Earthquake Engineering*, 2004.
[35] Applied Technology Council (ATC), Quantification of Building Seismic Performance Factors (FEMA P-695), 2009.
[36] J. W. Baker, C. A. Cornell, A vector-valued ground motion intensity measure consisting of spectral acceleration and epsilon, *Earthq. Eng. Struct. Dyn.*, 34(10), 1193–1217, 2005.
[37] J. W. Baker, Efficient analytical fragility function fitting using dynamic structural analysis, *Earthq. Spectra*, 31(1), 579–599, 2015,
[38] W. Muñoz, M. Mohammad, A. Salenikovich, P. Quenneville, Determination of Yield Point and Ductility of Timber Assemblies: in Search for a Harmonised Approach, *Meeting 41 of CIB-W18*, 2008.

https://doi.org/10.52202/069179-0337